Redshifted intergalactic ^{3}He$^+$ 8.7 GHz hyperfine absorption

Matthew McQuinn*
Harvard-Smithsonian Center for Astrophysics, 60 Garden St., Cambridge, MA 02138, USA

Eric R. Switzer†
Kavli Institute for Cosmological Physics, The University of Chicago, Chicago, IL, 60637, USA
(Dated: January 6, 2010)

Motivated by recent interest in redshifted 21 cm emission of intergalactic hydrogen, we investigate the 8.7 GHz $^2S_{1/2}$ $F = 0 - 1$ hyperfine transition of ^{3}He$^+$. While the primordial abundance of ^{3}He relative to hydrogen is 10^{-5}, the hyperfine spontaneous decay rate is 680 times larger. Furthermore, the antenna temperature is much lower at the frequencies relevant for the ^{3}He$^+$ transition compared to that of $z > 6$ 21 cm emission. We find that the spin temperature of this 8.7 GHz line in the intergalactic medium is approximately the cosmic microwave background temperature, such that this transition is best observed in absorption against high-redshift, radio-bright quasars. We show that intergalactic 8.7 GHz absorption is a promising, unsaturated observable of the ionization history of intergalactic helium (for which He II→He III reionization is believed to complete at $z \sim 3$) and of the primordial ^{3}He abundance. Instruments must reach $\sim 1\,\mu$Jy RMS noise in bands of 1 MHz on a 1 Jy source to directly resolve this absorption. However, in combination with H I Lyα forest measurements, an instrument can statistically detect this absorption from $z > 3$ with $30\,\mu$Jy RMS noise in 0.1 MHz spectral bands over 100 MHz, which may be within the reach of present instruments.

PACS numbers: 95.30.Dr, 32.10.Fn, 98.62.Ra

arXiv:0905.1715v3 [astro-ph.CO] 6 Jan 2010

I. INTRODUCTION

The $^2S_{1/2}$ $F = 0 - 1$ hyperfine splitting of neutral hydrogen at 1.42 GHz has been the subject of intense study as an observable of the cosmological reionization of hydrogen. Several experiments aim to map the high-redshift 1.42 GHz emission, but another approach is to study the pre-reionization era in absorption against bright radio sources [1–3]. This approach is restricted to times when the spin temperature of intergalactic hydrogen is close to the cosmic microwave background (CMB) temperature ($z \gtrsim 15$) and may prove difficult because of the paucity of bright radio sources from this era.

Here, we propose a similar experiment using the ^{3}He$^+$ $^2S_{1/2}$ $F = 0-1$ hyperfine transition at 8.666 GHz [4, 5] in absorption. This proposal is motivated by the fact that, while the abundance of ^{3}He is $\sim 10^{-5}$ that of hydrogen, the spontaneous decay rate A_{10} is 680 times larger ($A_{10} = 1.95 \times 10^{-12}$ s^{-1} for ^{3}He$^+$ [6]) and because we find the spin temperature of this transition is close to that of the CMB, making $z \sim 3$ intergalactic 8.7 GHz emission very difficult to observe. We show that intergalactic 8.7 GHz absorption can be used as an observable of cosmological He II→He III reionization (hereafter, "He II reionization") and He I→He II reionization (which is believed to be concurrent with H I reionization). This absorption can also provide a handle on the abundance of ^{3}He from primordial nucleosynthesis.

The reionization of the hydrogen and helium in the intergalactic medium is one of the least understood events in our cosmic history. Observations of the Lyα forest constrain the intergalactic hydrogen to be reionized at $z > 6$. For any plausible astrophysical spectrum, if it ionizes the hydrogen, then helium also becomes at least singly ionized. However, it takes a hard source of ultraviolet radiation to doubly ionize the helium. Quasars are an intense source of such radiation, and their abundance peaks at $z \sim 3$. The present paradigm is that they finish doubly ionizing the helium at $z \sim 3$ [7–10]. However, helium becomes doubly ionized at the same time that hydrogen is reionized (at $z > 6$) in more exotic models, such as if dark matter annihilation byproducts [11] or black holes [12] ionize the hydrogen.

Several observations of the IGM suggest that He II reionization is ending at $z \sim 3$. Ricotti et al. [13] and Schaye et al. [14] measured the gas temperature from the widths of the narrowest lines in the H I Lyα forest and found an increase in the temperature of $\Delta T \sim 10^4$ K between $z = 3.5$ and $z = 3$ (before a decline at lower redshifts) that is likely due to the heating from He II reionization. In addition, observations of He II Lyα absorption at $2.8 < z < 3.3$ find 10s of comoving Mpc (cMpc) regions with no detected transmission [15], which may signify the presence of diffuse intergalactic He II [16]. Finally, Songaila [17] and Agafonova et al. [18] interpreted evolution in the column density ratios of certain highly ionized metals at $z \approx 3$ as evidence for He II reionization. However, all of these probes are quite indirect and their interpretation is controversial. The observable discussed in this paper, ^{3}He$^+$ hyperfine absorption, would be a more direct probe of He II reionization.

Observations of ^{3}He$^+$ hyperfine emission from H II regions are currently the most reliable method to constrain

*Electronic address: mmcquinn@cfa.harvard.edu
†Electronic address: switzer@kicp.uchicago.edu

primordial and stellar production of ^{3}He [5, 19, 20]. Such observations have constrained the fractional abundance of ^{3}He to be $1.5^{+1.0}_{-0.5} \times 10^{-5}$ [20], consistent with the Big Bang Nucleosynthesis value of $^3\mathrm{He/H} = 1.04 \pm .04 \times 10^{-5}$ implied by the best-fit WMAP cosmology [21]. These galactic ^{3}He$^+$ measurements require detailed modeling of H II regions and their emission lines. In addition, traditional models predict that stellar nucleosynthesis should produce a significant quantity of ^{3}He in excess of the primordial abundance. Surprisingly, in most H II regions, a significant excess is not found (e.g. [22, 23]). An intergalactic measurement of the ^{3}He would be much less contaminated by ^{3}He produced in stars, and such a measurement is likely required for a precision measurement of the primordial ^{3}He abundance.

Previous studies have mentioned ^{3}He$^+$ hyperfine transition as a potential cosmological observable [24–28]. Syunyaev [24] pointed out that this line exists and could potentially be used to constrain big bang nucleosynthesis. Sigurdson and Furlanetto [25] noted that it might be easier to observe than the 92 cm hyperfine line of intergalactic deuterium from the dark ages (the focus of their study) because of the reduced backgrounds, but, in followup, [26] asserted that detecting it would require a heroic effort.

This is the first study to consider the ^{3}He$^+$ hyperfine line in practical detail, and we find that this signal is more detectable than previously thought. This paper discusses the nature of the intergalactic 8.7 GHz signal, the sensitivity requirements of an observation to detect it, and this line's potential scientific applications. We find that neither spin-exchange collisions with electrons nor the scattering of He II Lyman-series photons in the $z \sim 3$ IGM are sufficient to decouple the ^{3}He$^+$ 8.7 GHz spin temperature significantly from the CMB temperature. This is in contrast to the 21 cm transition of hydrogen, where calculations find that the spin temperature is coupled to the kinetic temperature by the ambient radiation for $z \lesssim 15$ [26]. Because of the small spin temperature of intergalactic ^{3}He$^+$, it is easiest to observe this transition in absorption against radio-bright, high-redshift quasars.

For $2 < z < 6$, the ^{3}He$^+$ hyperfine line falls between 1.2 GHz and 2.9 GHz. This is a higher frequency range than that of redshifted 21 cm surveys, and is convenient for several reasons. First, the sky temperature (which represents the noise floor) at ~ 2 GHz is 4 K [29], which is much smaller (by a factor > 100) than that of $z > 6$ 21 cm emission. Frequencies of a couple GHz are also less susceptible to ionospheric fluctuations or galactic Faraday rotation than measurements at hundreds of MHz. Further, these frequencies are not high enough that the lowest major resonances from the atmosphere or from astrophysical sources interfere. We show that constraints on the ^{3}He abundance and He I reionization are formally within reach of a 10^5 m^2 interferometer, while a statistical detection of 8.7 GHz ^{3}He$^+$ absorption from during He II reionization could be feasible with existing instruments.

This paper calculates the strength of the ^{3}He$^+$ hyperfine absorption signal (Sec. II) and discusses its observability. Sec. III discusses the sensitivity requirements to detect this signal in absorption. Finally, Sec. IV argues that other redshifted lines which fall into this band are likely to be subdominant to the ^{3}He$^+$ 8.7 GHz absorption and shows that many relevant instrumental considerations are not as stringent as those to detect high-redshift 21 cm emission.

II. THE ^{3}He$^+$ SIGNAL

A. The optical depth

The $I = 1/2$ nuclear spin of ^{3}He$^+$ splits the ground state into an $F = 0$ singlet and an $F = 1$ triplet, but because the nuclear moment has the opposite sign relative to hydrogen, the singlet is the excited state [30]. The optical depth to redshift through the hyperfine line is [31]

$$\tau_{^3\mathrm{He}^+} = \frac{c^3 \hbar A_{10}}{16 k_\mathrm{B} T_\mathrm{s} \nu_{10}^2} \frac{n_{^3\mathrm{He}^+}}{(1+z) dv/dy}, \tag{1}$$

where $\nu_{10} = 8.7$ GHz, $n_{^3\mathrm{He}^+} = n_\mathrm{H} f_{^3\mathrm{He}} x_\mathrm{HeII} \Delta_b$, Δ_b is the gas density in units of the cosmic mean, v is the proper line-of-sight velocity (Hubble flow plus peculiar velocity), and y is the conformal distance. The spin temperature T_s determines the relative abundance of the hyperfine excited state to the ground state as $\exp[-h\nu_{10}/(k_\mathrm{B}\, T_\mathrm{s})]/3$, and x_HeII is the fraction of helium that is He II (and $\bar{x}_\mathrm{HeII}$ is its volume average). Lastly, $f_{^3\mathrm{He}}$ is the fractional abundance of ^{3}He relative to hydrogen, which we take to be 1.04×10^{-5}. This is the value for a ΛCDM cosmology with $\Omega_b = 0.046$, $\Omega_m = 0.27$, zero spatial curvature, massless neutrinos, a Hubble parameter of $h = 0.71$, and CMB temperature of $T_\mathrm{CMB} = 2.73\,(1+z)$ K [21]; we adopt this cosmological model throughout.

For a reference epoch, we take $z = 3.6$ (1.84 GHz, or 16.3 cm) where the fiducial model for He II reionization in [10] predicts $\bar{x}_\mathrm{HeII} \sim 0.5$, and this prediction derives mainly from the observed quasar luminosity function. With these choices, we can rewrite Eq. (1) as

$$\begin{aligned} \tau_{^3\mathrm{He}^+} &= 4.5 \times 10^{-7} x_\mathrm{HeII} \Delta_b \frac{T_\mathrm{CMB}(z)}{T_\mathrm{s}} \left(\frac{1+z}{4.6}\right)^{1/2} \\ &\times \left(\frac{H(z)/(1+z)}{dv/dy}\right). \end{aligned} \tag{2}$$

Note that in emission this transition has brightness temperature $(T_\mathrm{s} - T_\mathrm{CMB})\,\tau_{^3\mathrm{He}^+}$, which Sec. II B demonstrates is negligible for intergalactic ^{3}He$^+$. It is most promising to look for the intergalactic signature in absorption against bright continuum sources.

Systems that have overdensities greater than several have decoupled from the Hubble flow, and one can picture

these regions as a forest of discrete clouds. A cloud with column density $N_{^3\mathrm{He}^+}$ in $^3\mathrm{He}^+$ has

$$\tau_{^3\mathrm{He}^+} = 1.1\times10^{-5}\left(\frac{N_{^3\mathrm{He}^+}}{10^{15}\,\mathrm{cm}^{-2}}\frac{10\,\mathrm{K}}{T_\mathrm{s}}\frac{30\,\mathrm{km\,s}^{-1}}{\Delta v}\right), \quad (3)$$

where Δv is the velocity width of the cloud (including Doppler broadening). From the H I Lyα forest, we measure the neutral hydrogen column density N_HI of these clouds, so it is more intuitive to write Eq. (3) in terms of N_HI, rather than $N_{^3\mathrm{He}^+}$. If we assume that all the helium is He II, photoionization equilibrium for the hydrogen, and the analytic formula that maps N_HI to Δ_b given in Schaye [32] (valid for $N_\mathrm{HI}\lesssim10^{18}\,\mathrm{cm}^{-2}$ and which provides an excellent fit to numerical simulations), then the optical depth to 8.7 GHz absorption of a single structure can be written as

$$\begin{aligned}\tau_{^3\mathrm{He}^+} &\approx 3\times10^{-6}\left(\frac{N_\mathrm{HI}}{10^{15}\,\mathrm{cm}^{-2}}\frac{\Gamma_\mathrm{HI}}{10^{-12}\,\mathrm{s}^{-1}}\right)^{1/3} \quad (4)\\ &\times \left(\frac{10\,\mathrm{K}}{T_\mathrm{s}}\frac{30\,\mathrm{km\,s}^{-1}}{\Delta v}\right)\left(\frac{T}{2\times10^4\,\mathrm{K}}\right)^{0.5},\end{aligned}$$

where Γ_HI is the H I photoionization rate, which is measured to be $\Gamma_\mathrm{HI}\approx10^{-12}\,\mathrm{s}^{-1}$ at $z=2-5$ (e.g. [33]). Column densities of $10^{15}\,\mathrm{cm}^{-2}$ are commonplace in the H I Lyα forest (~1 per 10 cMpc at $z\approx3$).

B. The spin temperature

The brightness temperature of $^3\mathrm{He}^+$ emission scales as $(T_\mathrm{s}-T_\mathrm{CMB})/T_\mathrm{s}$, while the optical depth to absorption scales as $1/T_\mathrm{s}$. Therefore, whether the resonance is viewed in absorption or emission depends on how decoupled T_s is from T_CMB. The spin temperature of the hyperfine transition is primarily determined by: 1) radiative excitation at ν_{10}, 2) collisional spin exchange, 3) excitation by the radiation near He II Lyα and other allowed transitions (through the $^3\mathrm{He}^+$ equivalent of the Wouthuysen-Field effect) [34][82]. Appendix A summarizes additional, subdominant spin coupling mechanisms.

In equilibrium, the spin temperature is given by

$$T_\mathrm{s}^{-1} = \frac{T_\mathrm{CMB}^{-1}+x_\mathrm{c}T_\mathrm{k}^{-1}+x_\alpha T_\alpha^{-1}}{1+x_\mathrm{c}+x_\alpha}, \quad (5)$$

where T_k is the kinetic temperature, T_α is the effective color temperature of the resonant radiation, and the x's are coupling coefficients that are given below. Because of the large difference between T_k and T_α versus T_CMB, for relevant values of the x's Eq. (5) can be rewritten as

$$T_\mathrm{s}\approx T_\mathrm{CMB}\,(1+x_\mathrm{c}+x_\alpha). \quad (6)$$

Eq. (5) and Eq. (6) assume the CMB is the dominant background at ν_{10}. Seiffert et al. [35] found mild distortions to the CMB temperature from extragalactic emission at radio frequencies, but this emission is negligible at 8.7 GHz in the IGM at all redshifts [83].

1. Collisional spin exchange

Spin exchange from collisions with electrons dominates over spin exchange from collisions with ionic and atomic species, which have thermal velocities that are further suppressed relative to electrons by their masses. The collisional spin-exchange cross section derived from partial wave phase shifts from [36] is

$$\begin{aligned}\sigma(E) &= \frac{3\pi}{4k^2(E)}\sum_{\ell=0}^{\infty}(2\ell+1)\sin^2[\delta_\ell^t(E)-\delta_\ell^s(E)]\\ &\approx \frac{1.05}{k^2(E)}, \quad (7)\end{aligned}$$

where $\hbar k=\sqrt{2m_eE}$ is the wavenumber of the scattering electron and we have worked in the approximation that the phase shifts are constant over relevant energies (see Appendix B for additional discussion regarding Eq. 7). The parameter C in $\sigma(E)=C/k^2(E)$ has been evaluated at 1 eV, and it rises gradually to 1.08 at 8 eV. The s and p-wave shifts ($\ell=0$ and 1) dominate the summation in Eq. (7). In addition, the thermally averaged cross section is

$$\bar\sigma = \frac{1}{(k_\mathrm{B}T_\mathrm{k})^2}\int_0^\infty dE\sigma(E)Ee^{-E/(k_\mathrm{B}T_\mathrm{k})}\approx\frac{14.3\ \mathrm{eV}}{k_\mathrm{B}T_\mathrm{k}}a_o^2, \quad (8)$$

where a_o is the Bohr radius. The collisional coupling coefficient is then [37]

$$\begin{aligned}x_\mathrm{c} &= \frac{n_\mathrm{e}T_\star}{A_{10}T_\mathrm{CMB}}\sqrt{\frac{8k_\mathrm{B}T_\mathrm{k}}{\pi m_ec^2}}c\,\bar\sigma \quad (9)\\ &\approx 1.0\times10^{-2}\,\Delta_b\left(\frac{1+z}{4.6}\right)^2\left(\frac{T_\mathrm{k}}{10^4\,\mathrm{K}}\right)^{-1/2},\end{aligned}$$

where n_e is the electron density and the second line assumes that hydrogen is fully ionized and the helium is singly ionized. The temperature of the IGM is measured from the H I Lyα forest to be $\sim2\times10^4$ K near mean density at $z\sim2-4$ [13, 14]. Therefore, the collisional spin coupling will be weak at $z=3.6$ except in overdense regions ($\Delta_b\gtrsim100$ or $n_e\gtrsim3\times10^{-3}$ cm^{-3} for $x_\mathrm{c}>1$).

2. Radiative spin coupling

In addition to collisions, ultraviolet radiation produced by He III→He II recombinations and directly by quasars can penetrate into the He II regions and affect T_s by pumping the hyperfine states through electronic dipole transitions. This effect turns out to be weaker for the 8.7 GHz transition of $^3\mathrm{He}^+$ compared to the analogous mechanism for the 21 cm line of atomic hydrogen because A_{10} is much larger in the case of ^{3}He+ and because the radiation backgrounds are much weaker at the $^3\mathrm{He}^+$ allowed dipole transitions.

Photons that have energies greater than He II Lyα can redshift into the He II Lyα resonance or higher series

resonances. However, scattering off of the higher series resonances is not an important contribution to pumping ^{3}He$^+$ hyperfine states because such photons are removed by ^{4}He$^+$ before they redshift into the ^{3}He$^+$ resonances [38]: A He II Lyn photon scatters on average 5 times by ^{4}He$^+$ before being destroyed, and the optical depth for a photon that redshifts across the ^{4}He+ Lyα resonance is $\tau_{^4\mathrm{HeII,Ly}\alpha} = 4200\, x_{\mathrm{HeII}}\, \Delta_b\, [(1+z)/4.6]^{3/2}$ ($\tau_{^3\mathrm{HeII,Ly}\alpha} = 0.5\, x_{\mathrm{HeII}}\, \Delta_b\, [(1+z)/4.6]^{3/2}$ for the ^{3}He+ Lyα resonance). Approximately 0.3 of each destroyed Lyn photon for $n > 2$ ends up as a He II Lyα photon, which contributes to the pumping [39, 40].

Coupling of the spin temperature to the color temperature of the radiation at ^{3}He$^+$ Lyα is described by the coefficient [39, 41, 42]

$$x_\alpha = \frac{P_{10} T_\star}{A_{10} T_{\mathrm{CMB}}} = \frac{16\pi \chi^\alpha_{\mathrm{HeII}} T_\star}{9 A_{10} T_{\mathrm{CMB}}} \beta_\infty S_\alpha = \frac{\beta_\infty}{\beta_\alpha} S_\alpha, \quad (10)$$

where

$$\beta_\alpha = 9.6 \times 10^{-10} \left(\frac{1+z}{4.6}\right)\ \mathrm{cm^{-2}\,Hz^{-1}s^{-1}sr^{-1}}, \quad (11)$$

$P_{10} = (4/9)\, P_{\alpha,{}^3\mathrm{He}^+}$ is the scattering de-excitation rate [84], $P_{\alpha,{}^3\mathrm{He}^+} \equiv 4\pi \chi^\alpha_{\mathrm{HeII}} \beta_\infty S_\alpha$ is the He II Lyα scattering rate, $\chi^\alpha_{\mathrm{HeII}} = \pi e^2/(m_e c) f_\alpha$ is the He II Lyα cross section with oscillator strength $f_\alpha = 0.416$, and $k_{\mathrm{B}} T_\star \equiv h\nu_{10}$. The function $S_\alpha \equiv \int d\nu \phi(\nu) \beta(\nu)/\beta_\infty$ (where $\phi(\nu)$ is the absorption profile normalized such that $\int d\nu \phi(\nu) = 1$) describes the shape of the spectrum near resonance. The spectrum is not changed significantly around resonance at relevant T_{K} such that $S_\alpha \approx 1$.

Lyα scattering off of ^{4}He+ rather than ^{3}He+ shapes the spectrum of the radiation at the ^{3}He$^+$ Lyα resonance, which is offset 14 km s^{-1} redward of the ^{4}He+ Lyα resonance or a few ν_D for 10^4 K gas, where ν_D is a Doppler width of ^{4}He+. In the absence of redshift, repeated scattering off of ^{4}He+ creates a "mesa" absorption profile in the incident spectrum centered on ^{4}He+ Lyα with half-width $(2 \log \tau_{^4\mathrm{HeII,Ly}\alpha})^{1/2}\, \nu_D \sim 4\, \nu_D$ [34]. Redshifting helps to extend the mesa profile across the ^{3}He+ Lyα resonance. Energy exchange with the gas during scattering causes the slope of the flat part of the mesa to converge to that of the Planck function with temperature equal to T_{k} [34], but whether $T_\alpha \approx T_{\mathrm{k}}$ at the ^{3}He+ resonance depends on the temperature, ionization state, and density of the gas. Furthermore, absorption of ultraviolet photons by the 3d $^3\mathrm{P}^0_2$–2P^2 $^3\mathrm{P}_2$ resonance of O III that falls 9 km s^{-1} redward of ^{3}He+ Lyα can also deplete the flux redward of this resonance [43]. This effect can drive T_s to negative values [43]. Although, this effect has only been considered for oxygen abundances that are orders of magnitude larger than the mean IGM abundance. Because of these considerations, a detailed treatment is required to determine T_α. Fortunately, such a treatment is not required for this study because we find $x_\alpha \ll 1$. However, even if x_α were near unity, the value of T_α would not be important for determining T_s except in locations where T_α is fine-tuned such that $|T_\alpha| \lesssim T_{\mathrm{CMB}}$, which is unlikely.

Scatterings from He II Lyα photons produced by recombinations pump the 8.7 GHz transition. However, a He III→He II recombination must take place $\sim .1$ cMpc from the edge of the He II region in order for any He II Lyα photon that results to be able to reach the He II region edge before redshifting off resonance [85]. Therefore, only if the He II region contains some He III gas (or if the recombining gas is near the He II region) are He II Lyα photons produced by recombinations present. It is likely that a large fraction of the ionizing photons during He II reionization have long mean free paths and can penetrate deep into He II regions, producing He III [10, 44].

An estimate for the specific intensity (in units of cm^{-2}s^{-1}Hz^{-1}sr^{-1}) at He II Lyα from *in situ* recombinations is

$$\beta_\infty\Big|_{\mathrm{rec}} \approx 0.7\, \frac{c\, \alpha_B(T) \bar{n}_e \bar{n}_{\mathrm{He}}}{4\pi} \langle \Delta_b^2 x_{\mathrm{HeIII}} \rangle \left|\frac{dt}{dz}\frac{dz}{d\nu}\right| \quad (12)$$
$$\approx 6 \times 10^{-13} \left(\frac{1+z}{4.6}\right)^{9/2} \left(\frac{T}{10^4 \mathrm{K}}\right)^{-0.7} \langle \Delta_b^2 x_{\mathrm{HeIII}} \rangle,$$

where α_B is the Case B He II recombination coefficient, and 0.7 represents the ≈ 0.7 Lyα photons, on average, that each He III→He II recombination produces [45]. The brackets signify the average over the diffusion scale [this scale must be smaller than the total distance a photon travels as it redshifts across resonance or $0.1(\Delta v/10\,\mathrm{km\,s^{-1}})$ cMpc and larger than $\tau^{-1/2}_{^4\mathrm{HeII,Ly}\alpha}$ times this distance]. The value of $\langle \Delta_b^2 x_{\mathrm{HeIII}} \rangle$ in most intergalactic He II regions is less than unity because $\Delta_b \sim 1$ and $x_{\mathrm{HeIII}} \ll 1$. In the simulations of McQuinn et al. [10], at the time that 50% of the helium in the IGM is He II, the mean values of x_{HeIII} in He II regions is ~ 0.1 (and becomes ~ 0.3 when there is net 80% ionization of He II). Assuming $x_{\mathrm{HeIII}} = 0.5$, the required value of Δ_b such that $x_\alpha \gtrsim 1$ is $\Delta_b \gtrsim 40$ at $z = 3.6$. Therefore, recombinations are not sufficient except in very overdense regions to decouple T_{S} from T_{CMB}.

Higher series Lyman photons can also pump this transition. However, only a small fraction $n > 2$ He II Lyman series photons are converted into Lyα photons, and their contribution to β_∞ is much smaller than direct He II Lyα production from recombinations (see [86]).

Ultraviolet photons with energies greater than 40.8 eV and less than 54 eV that are produced by quasars can also pump the ^{3}He$^+$ hyperfine states since these photons will redshift into the HeII Lyman resonances. (Stars in galaxies produce very few photons with energies greater than 40.8 eV.) Because quasar spectra should not vary significantly over this wavelength interval, the radiation that redshifts onto resonances is a fairly homogeneous background. (Note that a photon redshifting from He II Lyβ to He II Lyα travels $600[(1+z)/4.5]^{1/2}$ cMpc.) However, detailed estimates for the UV background from quasars in [46] find $\beta \lesssim 10^{-12}\,\mathrm{s^{-1}cm^{-2}\,Hz^{-1}\,sr^{-1}}$ in this band, which is insufficient to significantly decouple T_s

from $T_{\rm CMB}$ [87].

In summary, we find that $T_{\rm s} \sim T_{\rm CMB}$ except in regions dense enough for collisional coupling to be important ($\Delta_b \gtrsim 100$ at $z = 3.6$ for $x_c = 1$) or in dense regions where radiative coupling can operate ($\Delta_b \gtrsim 40$ at $z = 3.6$ for $x_\alpha = 1$). In contrast, galactic detections of $^3{\rm He}^+$ from H II regions have found the 8.7 GHz line of $^3{\rm He}^+$ in emission. There, though, the electron number density is $\sim 10^8$ times higher than in the $z \sim 3$ IGM.

Because the $T_{\rm s}$ does not decouple significantly from $T_{\rm CMB}$, detecting intergalactic $^3{\rm He}^+$ 8.7 GHz emission during this era would require a mammoth effort. Even if one were to take $T_{\rm s} \gg T_{\rm CMB}$ for all the $^3{\rm He}^+$ gas in the universe, we find that sensitivities of ~ 0.3 μK at ~ 10 cMpc scales would be required. However, because we showed that $T_{\rm s} \approx T_{\rm CMB}$ except in and near galaxies, the sensitivity requirements are at least a factor of several more stringent. Simple estimates suggest that this small signal still could be detected with the Square Kilometer Array. However, it is not clear that $^3{\rm He}^+$ is the dominant emission line at ~ 2 GHz and, for example, 4.2 GHz hyperfine emission from ^{14}NV may be more important (Sec. IV B 1), and 21 cm emission will dominate over the $^3{\rm He}^+$ emission signal from $z > 5.1$. Detecting the $^3{\rm He}^+$ 8.7 GHz line in absorption is the focus for the remainder of this paper.

III. PROSPECTS FOR DETECTION

Fig. 1 shows an estimate for the $^3{\rm He}^+$ absorption signal along four 190 cMpc skewers and at four times during He II reionization. Each skewer is calculated from the L1 simulation in [10], assuming that $T_{\rm s} = T_{\rm CMB}$. He III regions can be identified from these skewers (the regions in which most pixels have zero flux). Note that these calculations do not capture the densest, most absorbed regions during He II reionization, which may remain self-shielded after He II reionization. After He II reionization, estimates are that there will be ~ 1 self-shielding system per 30 cMpc (e.g., [47]). In addition, the ionizing radiation from the observed quasar will decrease the amount of absorption close to it, a "$^3{\rm He}^+$ proximity effect". This effect is not included in Fig. 1 and may prove valuable for probing the He II reionization process.

In this section, we first discuss the high-redshift, radio-bright source population (Sec. III A) and then quantify the prospects for detecting the 8.7 GHz absorption signal with existing and planned radio telescopes (Sec. III B). We discuss three methods to detect the signal: (1) direct imaging of 8.7 GHz absorption, (2) a statistical detection of it, and (3) a targeted observation that uses the quasar's Lyα forest absorption to locate regions with large $\tau_{^3{\rm He}^+}$. We quantify the telescope specifications required to detect the signal with each of these methods. This section discusses only the formal sensitivity limit from thermal radiometer noise, and Sec. IV A describes important instrumental factors.

A. The high-redshift, radio-bright quasar population

Radio-bright quasars represent $\sim 10\%$ of the quasar population, and their abundance peaks at $z \sim 2.5$ [48–50]. The radio quasars described here are also optically luminous, allowing a determination of their redshift [48]. We use the fact they are optically luminous in Sec. III B 3 to consider the H I Lyα signal in parallel. Many radio observations have identified and studied these rare objects [48, 49, 51–53]. Taken together, surveys for radio-bright quasars cover a significant fraction of the sky, but are heterogeneous in flux limits, completeness, area, and spectroscopic followup in the optical. It is therefore challenging to estimate space densities of this population.

We found 17 sources with $z > 2$ and 1.4 GHz fluxes $\gtrsim$ 200 mJy from recent radio-bright quasar catalogs [48, 49, 51, 54]. Our selection is not complete, and is only meant to indicate that such sources exist. In the $z \sim 3.5$ range, the luminous "GHz peaked" [54] source J1445+0958 at $z = 3.53$ with ~ 2 Jy at 1.4 GHz is very promising (one also has PMN J1230-1139 at $z = 3.53$ with 480 mJy at 1.4 GHz and PMN J2003-3252 at $z = 3.78$ with 470 mJy at 1.4 GHz). At lower redshifts, one finds sources such as J0240-2309 at $z = 2.23$ with ~ 5 Jy at 1.4 GHz and several other $z \sim 2.3$ sources with ~ 2 Jy at 1.4 GHz [54]. At the high redshift end, the $z = 5.11$ quasar TN J0924-2201 has a flux of 70 mJy at 1.4 GHz [52, 53].

B. Sensitivity

1. *Directly resolving the* $^3{\rm He}^+$

The RMS thermal noise for an interferometric measurement of the flux of a point source is

$$\Delta S \approx \frac{2 k_{\rm B}\, \gamma\, T_{\rm sys}}{A_{\rm eff}\sqrt{2\, t_{\rm obs}\, \Delta\nu}} = 0.5\ \mu{\rm Jy}\cdot\gamma\left(\frac{T_{\rm sys}}{20\,K}\frac{10^5{\rm m}^2}{A_{\rm eff}}\right)\left(\frac{\rm week}{t_{\rm obs}}\frac{\rm MHz}{\Delta\nu}\right)^{\frac{1}{2}} \quad (13)$$

where $A_{\rm eff}$ is the effective collecting area of the interferometer, γ encodes the instrumental efficiency, $\Delta\nu$ is the width of the frequency channel, $t_{\rm obs}$ is the integration time, and $T_{\rm sys}$ is the system temperature of the instrument. Instruments that can currently operate at 2 GHz achieve system temperatures of 20–30 K, which is set by receiver noise rather than the sky ($T_{\rm sky} \approx 4$ K).

To directly resolve this absorption in mean density gas at $z = 3.6$ with a week-long observation, an ideal instrument with $A_{\rm eff} = 10^4\,{\rm m}^2$ requires a source with $S_{1.8{\rm GHz}} = \Delta S/\tau_0 \approx 10$ Jy (roughly five times the flux of any known $z \sim 4$ source), where τ_0 is the $^3{\rm He}^+$ optical depth for mean density gas in the Hubble flow. Here we

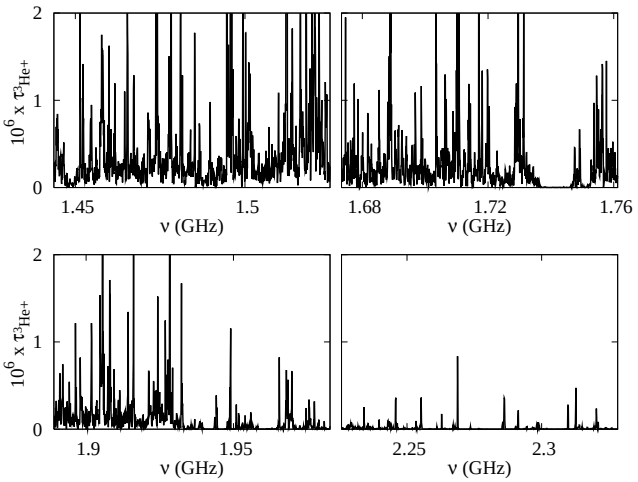

FIG. 1: The $^3He^+$ absorption signal along four 190 cMpc skewers at different times during He II reionization, calculated from simulation L1 in [10]. The top-left panel is from $\bar{z} = 5.0$ and volume-averaged He II fraction of $\bar{x}_{\rm HeII,V} \approx 0.9$, the top-right is from $\bar{z} = 4.2$ and $\bar{x}_{\rm HeII,V} \approx 0.7$, the bottom-left is from $\bar{z} = 3.6$ and $\bar{x}_{\rm HeII,V} \approx 0.4$, and the bottom-right is $\bar{z} = 2.9$ and $\bar{x}_{\rm HeII,V} \approx 0$. Note that these simulations do not resolve the densest peaks, where $\tau_{^3He^+}$ is largest.

have considered $10^4\,{\rm m}^2$ to be representative of existing telescopes [88], where in the bands we consider: 1) the GBT has $A_{\rm eff} \sim 5500\,{\rm m}^2$, 2) the GMRT ($\nu < 1.45$ GHz) has $A_{\rm eff} \sim 18200\,{\rm m}^2$ and, 3) the VLA has $A_{\rm eff} \sim 7300\,{\rm m}^2$. For contrast, the Square Kilometer Array (SKA) would require a source with only $S_{1.8{\rm GHz}} \approx 100$ mJy to image this signal. Overdensity (and infall) can boost the absorption and reduce these requirements.

Sensitivities of $\Delta S \approx 1\,\mu$Jy in 1 MHz spectral bins have not been achieved at these frequencies. For example, Omar et al. [55] performed a 5 hr observation on the Very Large Array at 1.7 GHz in search of OH absorption along a sightline, and they achieved $\approx 100\,\mu$Jy RMS per MHz, a factor of 100 off the mark for directly resolving the $^3He^+$ signal. However, we show in subsequent sections that clever methods can relax the sensitivity requirements to detect this absorption to $\Delta S \approx 30\,\mu$Jy in spectral bins of 0.1 MHz.

2. *Detecting the power spectrum of* 8.7 *GHz absorption*

The power spectrum of $\tau_{^3He^+}$ provides the simplest statistical description of the 8.7 GHz absorption. To calculate the sensitivity of an instrument to the power spectrum, we need to estimate the power spectrum of the instrumental noise. The power spectrum of the noise can be derived by equating $k_{\rm N}\,P(k)/\pi$ with ΔS^2, and is equal to

$$P_N(k) = \Delta S^2 \Delta\nu \frac{dy}{d\nu}, \tag{14}$$

where k is the wavevector in comoving units and $k_{\rm N}$ is the Nyquist wavevector, and where, for redshifts at which $\Omega_m(z) \approx 1$,

$$\frac{dy}{d\nu} \approx 2\left(\frac{z+1}{4.5}\right)^{1/2}\ {\rm cMpc}\cdot{\rm MHz}^{-1}. \tag{15}$$

If $P_N(k) < P_\tau(k)$, where P_τ is the power spectrum of $\tau_{^3He^+}(\nu)$, one can image individual k-modes.

The signal-to-noise (S/N) ratio of a statistical detection of P_τ is given by

$$\left(\frac{S}{N}\right)^2 = \frac{1}{2}\sum_{\rm modes}\left(\frac{P_\tau(k)}{P_\tau(k) + P_N(k)/S^2}\right)^2. \tag{16}$$

Eq. (16) assumes Gaussianity. The noise should be Gaussian, but the signal will not be. When the signal is comparable to the noise, Eq. (16) is an overestimate.

The S/N scales with experimental parameters (in the limit that radiometer noise dominates over sample variance) as

$$\frac{S}{N} \propto \frac{B^{1/2}\,A_{\rm eff}^2\langle S^2\rangle\,N_{\rm QSO}^{1/2}\,t_{\rm obs}}{\gamma^2\,\Delta\nu^{1/2}\,T_{\rm sys}^2}, \tag{17}$$

where $N_{\rm QSO}$ is the number of quasars in which this absorption is observed, B is the bandwidth, and Eq. (17) assumes that P_τ is independent of k (which is approximately true for $k \lesssim 10$ cMpc^{-1}).

The top panel in Fig. 2 shows P_τ at 4 times during the L1 simulation of He II reionization presented in [10] under the assumption $T_{\rm s} = T_{\rm CMB}$ (which is an excellent approximation; Sec. II B). It is clear that the amplitude changes during He II reionization, but the shape does not evolve considerably, even though the He III bubbles grow substantially over the redshift range considered. Aliasing makes the growth of bubbles less apparent in the 1-D power spectrum (and other statistics may be better suited to discriminate the bubble growth and structure). The "imaging" curve in Fig. 2 is the sensitivity of an observation with $\Delta S/S = 10^{-6}$ at 1 MHz (Eq. 14), and the "statistical' curve is the error on P_τ in bins of $\Delta k/k = 0.3$ for an observation with $B = 100$ MHz (including the cosmic variance term using the signal from $z \approx 3.6$).

The bottom panel in Fig. 2 calculates the S/N ratio (including cosmic variance) for different sensitivities in 1 MHz spectral bins assuming $B = 100$ MHz and using the $z = 3.6$ signal shown in the top panel. This panel demonstrates that an observation with $\Delta S/S = 10^{-6}$ in 1 MHz pixels is required to detect P_τ at $S/N \sim 3$ and that an observation that is twice as sensitive yields most of the available information (compare the $\Delta S/S = 5\times10^{-7}$ curve with the $\Delta S/S = 0$).

3. *A guided observation that uses the Ly*α *forest*

The sensitivity requirements to detect intergalactic 8.7 GHz absorption are relaxed if the Lyα forest absorption (as well as Lyβ and Lyγ) can also be measured for

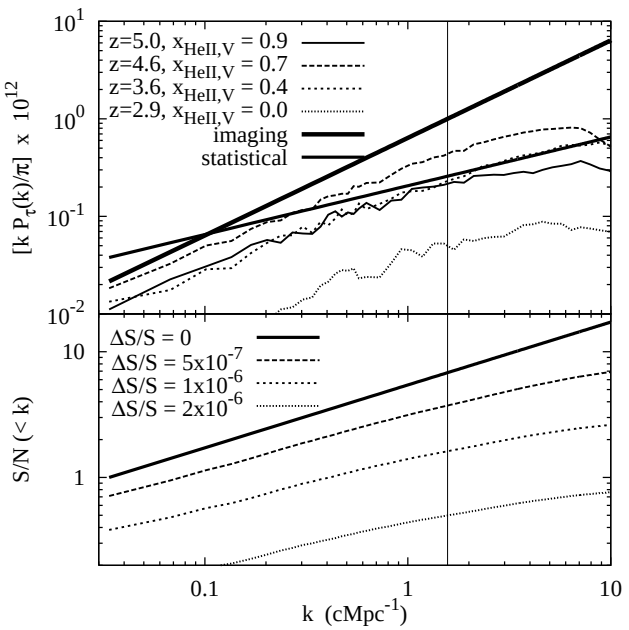

FIG. 2: Top panel: The power spectrum of $\tau_{^3\mathrm{He}^+}$ at several times during He II reionization, estimated from the L1 simulation of He II reionization presented in [10]. Also included is the noise power spectrum (the curve labeled "imaging"), assuming an observation with $\Delta S/S = 10^{-6}$ at 1 MHz over $B = 100$ MHz. If the noise power is smaller than $P_{\tau_{^3\mathrm{He}^+}}$, individual modes in the signal can be imaged. The "statistical" curve is the error on P_τ in a bin of size $\Delta k/k = 0.3$. The vertical line corresponds to the Nyquist wavevector for 1 MHz spectral resolution. Bottom Panel: The cumulative S/N ratio as a function of wavevector for the $z = 3.6$ signal shown in the top panel, assuming $B = 100$ MHz and the specified $\Delta S/S$ in 1 MHz spectral bins.

the same intergalactic systems. Lyman-series absorption reveals where the densest regions in the IGM lie, such that the signal can be measured just from the pixels in which the S/N ratio is expected to be highest. This strategy can result in a large gain in an observation's sensitivity to 8.7 GHz absorption. In Sec. III B 2, we saw that an observation with $\Delta S/S \sim 10^{-6}$ for $\Delta\nu = 1$ MHz was needed to detect this signal. Here we show that $\Delta S/S \approx 3 \times 10^{-5}$ for $\Delta\nu = 0.1$ MHz in combination with Lyα forest data can yield a significant detection of gas that will be ionized by He II reionization, and in Sec. III B 4 we show that dense systems could provide an even larger signal.

Using the H I Lyα forest as a template, an optimistic estimate for the S/N ratio that an observation of 8.7 GHz absorption can achieve is

$$\left(\frac{S}{N}\right)^2_{\rm opt} = \bar{x}^2_{\rm HeII}\,\Delta z \int_{N_{\rm HI}^{\rm min}}^{N_{\rm HI}^{\rm max}} \frac{{\rm d}^2\,{\rm N}}{{\rm d}z N_{\rm HI}} \left(\frac{S\,\tau_{\Delta\nu}}{\Delta {\rm S}}\right)^2 dN_{\rm HI}, \tag{18}$$

where ${\rm d}^2{\rm N}/{\rm d}z N_{\rm HI} \approx 3 \times 10^7\, N_{\rm HI}^{-1.5}\,(1+z)^{2.46}$ is the column-density distribution of $N_{\rm HI}$ using the fit in [56] valid for $z > 1.7$ and $N_{\rm HI} < 2 \times 10^{17}$ cm^{-2}, $N_{\rm HI}^{\rm min}$ and $N_{\rm HI}^{\rm max}$ are the minimum and maximum H I column densities included in the measurement, and Δz is the redshift interval that the observation spans. In addition, $\tau_{\Delta\nu} \approx \sigma_{^3\mathrm{He}^+} N_{^3\mathrm{He}}/\Delta\nu$, where $\sigma_{^3\mathrm{He}^+} = c^2 h A_{10}/(32\pi\nu_{10} k_B T_{\rm CMB})$, is the effective optical depth to the 8.7 GHz hyperfine transition if the absorber falls within a spectral pixel of width $\Delta\nu$ and has $x_{\rm HeII} = 1$. Finally, we assume $\Gamma_{\rm HI} = 10^{-12}$ s^{-1} [33] and we use the same mapping between $N_{\rm HI}$ and $N_{^3\mathrm{He}^+}$ used to derive Eq. (5), which yields the scaling $N_{^3\mathrm{He}^+} \propto N_{\rm HI}^{1/3}$.

Equation (18) is an estimate for the average S/N ratio that an observation of 8.7 GHz absorption can achieve, assuming that the location of all absorbers with $N_{\rm HI}$ between $N_{\rm HI}^{\rm max}$ and $N_{\rm HI}^{\rm min}$ is known (via the Lyman forest). In practice, the H I Lyα forest saturates easily (and the other Lyman resonances are contaminated by absorption from Lyα absorption at lower redshift and span a smaller redshift interval) such that it is difficult to discriminate between absorbers with $N_{\rm HI}$ in the range 10^{14}–10^{19}cm^{-2}.

A more realistic estimate for the S/N ratio may be to assume that an observation co-adds the radio signal from the location of dense absorbers with $N_{\rm HI} > N_{\rm HI}^{\rm min}$ (i.e., does not use knowledge about the value of $N_{\rm HI}$). In this case, an estimate for the S/N ratio at which ^{3}He$^+$ 8.7 GHz absorption can be detected is

$$\left(\frac{S}{N}\right)^2_{\rm cons} = \frac{\bar{x}^2_{\rm HeII}\,\Delta z}{\Delta S^2} \left(\int_{N_{\rm HI}^{\rm min}}^{N_{\rm HI}^{\rm max}} \frac{{\rm d}^2{\rm N}}{{\rm d}z N_{\rm HI}}\,(S\,\tau_{\Delta\nu})\,dN_{\rm HI}\right)^2 \times \left(\int_{N_{\rm HI}^{\rm min}}^{N_{\rm HI}^{\rm max}} \frac{{\rm d}^2{\rm N}}{{\rm d}z N_{\rm HI}}\,dN_{\rm HI}\right)^{-1}. \tag{19}$$

Therefore, equation (18) represents an $N_{\rm HI}$-weighted estimate for the S/N ratio and equation (19) represents an unweighted estimate.

Lyα forest absorbers with $N_{\rm HI} > 10^{13}$ cm^{-2} have widths of order $10 - 60$ km s^{-1} [56, 57]. Note that $\Delta\nu = 100$ kHz at 2 GHz corresponds to 15 km s^{-1}. Lines with $N_{\rm HI} > 10^{15-16}$ cm^{-2} will self-shield even after He II reionization [10] and have optical depths of unity to He II Lyman-limit photons. Systems that are moderately self-shielded are still highly ionized, such that it is likely safe to consider absorbers with $N_{\rm HI}^{\rm max} \lesssim 10^{16}$ cm^{-2} as probing He II reionization. Also, note that $\Delta_b \approx 150\,(N_{\rm HI}/10^{17}\ {\rm cm}^{-3})^{2/3}$ in the assumed model [32], such that $x_c \approx 1$ for $N_{\rm HI} = 10^{17}$ cm^{-3}. Therefore, electron collisions increase T_s by a factor of 2 over $T_{\rm cmb}$ at this column density and by a larger factor above it, reducing $\tau_{^3\mathrm{He}^+}$.

Fig. 3 shows our optimistic (dashed curves; Eq. 18) and conservative (solid curves; Eq. 19) estimates for the significance that ^{3}He$^+$ 8.7 GHz absorption could be detected with this method if $\bar{x}_{\rm HeII} = 1$. We assume for this calculation $z = 3.6$, $B = 100$ MHz ($\Delta z \approx 0.25$), and $N_{\rm HI}^{\rm min} = 10^{13}$ cm^{-2} (thin curves) or $N_{\rm HI,min} = 10^{14}$ cm^{-2} (thick curves). Both the optimistic and conservative estimates yield similar results, namely that $\Delta S \sim 30\,\bar{x}_{\rm HeII}$ μJy is required to detect the 8.7 GHz absorp-

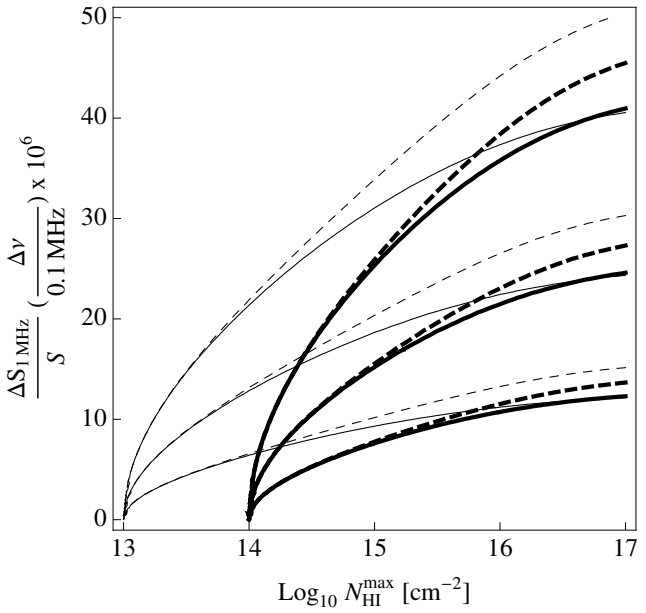

FIG. 3: Contours for 3, 5 and 10 σ detections in the $N_{\rm HI}^{\rm max}$ versus $[\Delta S/S\ (\Delta\nu/0.1\,{\rm MHz})]$ plane. The dashed curves are for the optimistic estimator and the solid are the conservative one. We assume for this calculation $z = 3.6$, $N_{\rm HI}^{\rm min} = 10^{13}$ cm^{-2} (thin curves) or $N_{\rm HI}^{\rm min} = 10^{14}$ cm^{-2} (thick curves), that $\bar{x}_{\rm HeII} = 1$, and $B = 100\,{\rm MHz}$.

tion signal using absorbers with $N_{\rm HI} \lesssim 10^{16}\,{\rm cm}^{-2}$ for $S = 1$ Jy. Also, note that it becomes easier to use the H I Lyα forest absorption to find dense regions as the redshift decreases (and the forest becomes more transparent), and it would be difficult to use this absorption to guide 8.7 GHz absorption studies at $z \gtrsim 5$ where only underdense regions are unsaturated.

Fig. 3 shows that observations with $\Delta S/S \gtrsim 2\times10^{-5}$ are most sensitive to the highest column density lines ($N_{\rm HI} \gtrsim 10^{16}\,{\rm cm}^{-2}$). However, for such observations there will be significant sightline-to-sightline scatter in the significance of a detection: There are ~ 1 systems with $N_{\rm HI} > 10^{17}{\rm cm}^{-2}$ per 100 MHz and this number scales as $N_{\rm HI}^{-0.5}$ with $N_{\rm HI}$.

4. ^{3}He$^+$ *absorption in super Lyman-limit and damped Lyα systems*

Thus far we have focused mostly on ^{3}He$^+$ absorption in intergalactic absorption systems with $N_{\rm HI} \lesssim 10^{16}\,{\rm cm}^{-2}$. Higher column-density systems are not as affected by He II reionization. However, clouds with $N_{\rm HI} \gtrsim 10^{20}$ cm^{-2} (called "DLAs") are easily identifiable in the H I Lyα forest because the damping wings of the hydrogen line appear in absorption. There will be ~ 1 such system per unit redshift at $z \approx 3$ [56].

These systems may make the easiest targets to search for large values of $\tau_{^3{\rm He}^+}$, and, since they will appear in absorption even after He II reionization, programs that aim to find redshifted ^{3}He$^+$ absorption may find the most immediate success if they target low-redshift DLAs, utilizing the brightest extragalactic radio sources on the sky.

It is thought that between $N_{\rm HI} \sim 10^{17}\,{\rm cm}^{-2}$ and $N_{\rm HI} \sim 10^{21}\,{\rm cm}^{-2}$, the nature of these absorbers shifts from being overdense intergalactic regions to being systems that live within halos and in galactic disks. Unfortunately, systems with $N_{\rm HI} \gtrsim 10^{18}\,{\rm cm}^{-2}$ are not as well-understood as those with lower $N_{\rm HI}$ because hydrodynamic simulations of the IGM do not include the detailed radiative transfer needed to model the ionization state of dense, self-shielding systems. It is not obvious how much He II absorption is expected from these high column-density systems and such modeling is beyond the scope of this paper. It is possible that some dense systems have $\tau_{^3{\rm He}^+} \sim 10^{-4}$ (especially at low redshift where $T_{\rm CMB}$ is smaller). See footnote [89] for further discussion.

C. ^{3}He$^+$ absorption from $z > 5.1$

Lower redshift 21 cm emission contaminates the ^{3}He$^+$ signal at $z > 5.1$. A mere $10^8\,M_\odot$ in neutral hydrogen with 20 km s^{-1} circular velocity at $z = 0.3$ has $S \approx 5\,\mu$Jy. It is conceivable that this large contaminant could prohibit the use of ^{3}He$^+$ 8.7 GHz absorption at high redshift. The most obvious application for 8.7 GHz absorption is to study He I reionization (which should be concurrent with hydrogen reionization).

Fortunately, low-redshift 21 cm emission is confined to galaxies, and, therefore, a small enough interferometric beam may be able to peer through the holes in the galaxy distribution and detect this high-redshift 8.7 GHz absorption signal. The $z = 0$ H I luminosity function constructed with the HIPASS survey extends to galaxies that contain $10^7\,M_\odot$ in neutral hydrogen, with a number density of detected objects of order 0.1 cMpc^{-3} [58]. If we conservatively assume a galaxy number density of 1 cMpc^{-3}, to observe 8.7 GHz absorption at $z = 7$ (or 21 cm radiation from $z = 0.3$) requires a beam constructed with baselines of length ~ 1 km in order for 1 foreground galaxy on average to enter the beam per 10 MHz. In addition, if we assume that all galaxies have radius 10 kpc in this toy model, the ultimate limit that a long baseline observation could achieve is ~ 0.01 foreground 21 cm-emitting galaxy per 10 MHz.

Observations of reionization of the first electron of helium via ^{3}He$^+$ 8.7 GHz absorption would require a bright $z > 6$ source. It is possible that a bright enough population of sources exist. Carilli et al. [53] observed two $z = 5.2$ radio galaxies that had fluxes 74 mJy and 18 mJy at 1.4 GHz to search for high-redshift 21 cm absorption. These sources were also selected to have a soft spectral index, so it is possible that even brighter $z > 5$ sources exist at ~ 2 GHz. Under ideal conditions, a 1 week observation of a 50 mJy source with the SKA would be sensitive to 1 μJy absorption features.

IV. CONTAMINANTS

A. Instrumental sources of contamination

There are a few significant challenges to the proposed program of wideband precision spectrometry: 1) terrestrial radio frequency interference (RFI), 2) passband calibration and stability, 3) gain calibration across polarizations, 4) distortions owing to a turbulent ionosphere, and 5) the frequency dependence of the instrumental beam. While it is beyond the scope of this study to quantify the severity of these challenges, we argue that many of these challenges are less severe for observations of 8.7 GHz absorption compared to $z > 6$ 21 cm emission.

The relevant spectral band has many broadband transmissions and satellite downlinks, with only small regions formally limited to radio astronomy [90]. While geographic avoidance of sight lines is helpful [59], RFI presents significant challenges to a wideband measurement. Transmissions will also be a concern for redshifted 21 cm observations. Because observations of $^3He^+$ absorption will only target a small patch of the sky and can rely on the correlations between the longest baselines whereas the sensitivity of redshifted 21 cm observations is dominated by short baselines of $\lesssim 100$ m [60], it may be easier to control this systematic for 8.7 GHz absorption.

Passband calibration is another significant consideration. While the error from thermal noise decreases with the square root of the integration time, variations in the passband (caused by instrumental resonances, or variations in the spectrometer passband) represent an irreducible noise term that could remain after usual calibration techniques such as chopping on and off-source. Because the signal power spectrum spans a wide range of spatial wavevectors, statistical detection may benefit slightly if passband errors are restricted to particular frequencies or wavevectors.

A third systematic, gain differences between the two linear polarizations, could lead to spurious signal. This systematic is more severe for cosmological 21 cm observations. For an observation of 21 cm emission at 200 MHz over a bandwidth of 10 MHz, the polarization vector of the foregrounds will rotate 2 rad for rotation measure (RM) equal to $10^{-3}\,\mathrm{rad\,cm^{-2}}$ (a rough value for RM above the galactic plane [61]) whereas for 8.7 GHz emission at 2 GHz over 100 MHz it will rotate 0.02 rad. Therefore, such gain miscalibration will lead to more line-of-sight structure for redshifted 21 cm emission.

Fourth, the ionosphere will distort the signal on timescales that are as small as seconds. However, the ionospheric distortion is much smaller for redshifted 8.7 GHz absorption than that of redshifted 21 cm [62]. Deflections through the ionosphere are less than $4''$, compared to 0.16° at 250 MHz.

Finally, the beam of any instrument is a function of frequency, such that additional sources enter in the beam as the frequency decreases. If the beam is sufficiently smooth with frequency, any leakage from sources entering and exiting the beam will contribute a smooth component on top of the signal that can be subtracted off. Since the severity of this leakage enters as a $\Delta\nu/\nu$ effect, this systematic is also likely to be less of a concern for $^3He^+$ observations than for that of redshifted 21 cm: Redshifted 21 cm measurements are most sensitive to $\gtrsim 10$ cMpc modes for which $\Delta\nu/\nu \lesssim 100$ [60] whereas $^3He^+$ observations are sensitive to $\lesssim 1$ Mpc modes for which $\Delta\nu/\nu \gtrsim 1000$.

B. Line emission contaminants

Since the abundance of $^3He^+$ is not much larger than the universal abundance of certain metals, contamination from different lines is a considerable concern. Our galaxy is the strongest source for many of the possible contaminating lines. However, terrestrial and galactic transitions can in principle be masked in searches for the redshifted $^3He^+$ absorption [91]. Extragalactic lines are weaker, but cosmological redshift allows higher frequency transitions to fall into the desired range and smears their effect over a range in frequency. In what follows we argue that the most likely contaminants are subdominant to the $^3He^+$ signal.

1. Hyperfine transitions from metals

For hydrogenic hyperfine transitions, the wavelength depends on the inverse cube of Z [27, 28]. Therefore, hydrogen-like ($1s$) transitions are at much higher frequencies, and only lithium-like ($2s$), boron-like ($2p_{1/2}$), and sodium-like ($3s$) ionic states fall at frequencies that can contaminate the 8.7 GHz signal. There are a few effects that suppress these contaminants: (1) isotopes that have nuclei with non-zero spin are generally rare, (2) the abundances of metals is low (especially in the IGM at high redshift where the average metallicity is $\sim 10^{-3}$ Solar), and (3) generally only a fraction of the metals are in the ionization state that could contaminate the 8.7 GHz signal.

We find that the most threatening hyperfine lines are the 4.2 GHz transition of ^{14}NV ($A = 9.8 \times 10^{-14}\,s^{-1}$, with isotopic fraction of 99.6%, and mass fraction $1.3 \times 10^{-3}\,W\,\Omega_b$, where W is the abundance relative to Solar), the 5.6 GHz transition of ^{13}CIV ($A = 1.7 \times 10^{-13}\,s^{-1}$, 1.1%, $7.3 \times 10^{-5}\,W\,\Omega_b$), and the 5.0 GHz transition of ^{29}SiV ($A = 6.3 \times 10^{-13}\,s^{-1}$, 4.7%, $4.4 \times 10^{-5}\,W\,\Omega_b$). Of these transitions, ^{14}NV will be biggest concern. However, it should be a subdominant absorber to ^{3}He in the IGM because its Einstein-A is 20 times smaller and its number density is only comparable for $W = 0.1 \gg \langle W_{\rm IGM}\rangle$. Also, the spin temperature is probably coupled to the gas temperature for ^{14}NV (as well as for other non-hydrogen-like hyperfine transitions), suppressing its absorption (see [92]).

2. Radio recombination lines

Radiation emitted and absorbed through transitions in extremely excited states of hydrogen – radio recombination lines (RRLs) – has been considered as a possible contaminant for H I 21 cm radiation (e.g., [63]). The RRLs of H I fall at frequencies

$$\nu \approx 2\,\mathrm{GHz}\,\Delta n\,\left(\frac{n}{150}\right)^{1/3} \tag{20}$$

where n is the principal quantum number. If a line falls within a frequency channel of width $\Delta\nu$ it contributes an optical depth [64]

$$\tau_{\rm RRL} = 2{\times}10^{-10}\left(\frac{T_{\rm k}}{10^4\,\mathrm{K}}\right)^{-\frac{5}{2}}\left(\frac{\mathrm{EM}}{1\mathrm{cm}^{-6}\,\mathrm{pc}}\right)\left(\frac{\Delta\nu}{1\,\mathrm{MHz}}\right)^{-1}, \tag{21}$$

where we have assumed local thermodynamic equilibrium (LTE) and EM is the emission measure. Note that it can be dangerous to assume LTE for RRLs. Collisions drive the occupation number of the highest n states closest to LTE, but lower n states will often be depopulated relative to LTE. This inversion can lead to enhanced emission or absorption from the highest n states than in LTE (and even maser emission). However, Shaver [64] showed that the corrections from LTE are most important at lower frequencies than relevant here.

Hα surveys find that in the direction of the galactic poles EM $\sim 1\,\mathrm{cm}^{-6}\,\mathrm{pc}$ [65], and the contribution to the EM from extragalactic objects will be comparable. Studies of damped H I Lyα systems in the Lyα forest reveal that a typical sightline passes through the outskirts of a few galaxies [66], and so we expect $\langle\mathrm{EM}\rangle \sim 10\,\mathrm{cm}^{-6}\,\mathrm{pc}$. Therefore, $\tau_{\rm RRL}$ should be much less than $\tau_{^3\mathrm{He}^+}$. Note that a sightline may pass through a galactic H II region where $\tau_{\rm RRL}$ is much larger. However, because the typical size for the radio emitting region of a quasar is $\sim 1\,\mathrm{kpc}$, H II regions in an external galaxy can cover only a small fraction of the quasar radio beam.

RRL emission should also be unimportant. The radio recombination line emission from a 10 kpc disk at a distance of 1000 cMpc contributes 10^{-4} μJy when averaged over a 1 MHz pixel, assuming EM $= 1\,\mathrm{cm}^{-6}\,\mathrm{pc}$ for all sightlines that intersect the disk and $T_{\rm k} = 10^4\,\mathrm{K}$.

3. Molecular Lines

Rotational transition rates of molecules are generally many orders of magnitude higher than for $^3\mathrm{He}^+$. Fortunately, the lowest lying rotation lines of diatomic molecules rotation lines lie at $\gtrsim 50$ GHz, and would enter our $1-2$ GHz band at redshifts at which their abundance is negligible. However, the redshifted signal of hyperfine lines from OH at ~ 1.7 GHz [67] or rotational modes of polyatomic molecules like H_2CO at 4.83 GHz, CH_3OH at 6.67 GHz and 12.18 GHz, H_2O at 22.2 GHz [68], and NH_3 at 23.7 GHz fall into our band (although, the latter two transitions would originate from $z > 10$).

The abundance of polyatomic molecules even in molecular clouds is many orders of magnitudes lower than ^{3}He (with the exception of H_2O), and we find that their absorption signal is subdominant to $^3\mathrm{He}^+$ except where the sightline directly passes through a galaxy. At these intersections, OH absorption at rest frame frequencies of $1.5-1.7$ GHz is likely the biggest concern (contaminating the 8.7 GHz absorption for $z > 4$). Molecular emission lines from galaxies that enter the beam can also contaminate the signal, but we estimate that their signal is again unimportant if LTE holds.

However, these low frequency molecular lines are often not found to be in LTE and several such lines are associated with maser emission ($T_{\rm line} < 0$) and can be extremely bright. In particular, OH $^2\Pi_{3/2}$ state hyperfine transitions in galaxies from $z = 0-0.2$ are a possible contaminant of the $^3\mathrm{He}^+$ signal at $1.5-1.7$ GHz ($^3\mathrm{He}^+$ absorption at $4.1 < z < 5.1$). These masers are concentrated in massive galaxies that are ultra-luminous in the infrared (because far infrared radiation pumps these masers). A small enough interferometric beam avoids significant contamination from these rare galaxies, and the beam size requirements are much less stringent than to avoid low redshift 21 cm emission outlined in Sec. III C.

The other potentially important known molecular maser transition is the 6.67 GHz transitions of H_2CO. However, the only identified extragalactic H_2CO masers are in the Large Magellanic Cloud (with $L \approx 10^{-5} - 10^{-6}\,L_\odot$), and despite H_2CO maser searches toward M33 and strong OH maser galaxies, only upper limits have been placed on their luminosities [69].

4. Fine structure lines

Absorption by fine structure lines can occur from an electronic state with $n > 1$ provided it has no downward allowed $\Delta n \geq 1$ transitions, which would depopulate this state. We concentrate only on hydrogen because of its abundance. For hydrogen, only the 2S state meets the above criteria through the $2P_{3/2} \rightarrow 2S_{1/2}$ transition at 2.7 cm (10.9 GHz), which has spontaneous transition rate $A_{\rm FS} = 8.9 \times 10^{-7}\ \mathrm{s}^{-1}$ [70]. This transition can appear in absorption in H II regions (if the 2S state is pumped by recombinations or collisions) or in H I regions (if it is pumped with H I Lyman-β absorption followed by Hα emission). However, Dijkstra et al. [71] showed that the later mechanism is extremely inefficient. Furthermore, in an ionized IGM, the Gunn-Peterson optical depth for this transition is $\tau_{\rm FS} \sim 10^{-15}\,[(1+z)/4]^{9/2}\Delta_b^2$. Therefore, intergalactic $2P_{3/2} \rightarrow 2S_{1/2}$ absorption by hydrogen is completely negligible compared to that of 8.7 GHz $^3\mathrm{He}^+$.

In galactic H II regions, collisions and recombinations mediated by the higher densities will more efficiently pump the 2S state, and it is possible that $2P_{3/2} \rightarrow 2S_{1/2}$ absorption will exceed our signal. Along a sightline such

regions will be rare and will be associated with DLAs in the H I Lyα forest, allowing these absorbers to be masked.

V. CONCLUSIONS

We have considered the $^2S_{1/2}$ $F = 0-1$ 8.7 GHz hyperfine transition of $^3He^+$ as an observable of the ionization state, density structure, and composition of the intergalactic medium. Despite the $\sim 10^{-5}$ deficit in abundance of ^{3}He relative to hydrogen, this transition is compelling because of 1) the high spontaneous rate, which exceeds the 21 cm rate by a factor of 680, 2) the convenient frequency range over which the redshifted signal falls, which has much lower sky temperatures compared to the frequencies for $z \gtrsim 6$ 21 cm emission, and 3) the techniques needed to extract this signal are in sharp contrast with that of redshifted 21 cm emission.

We showed that collisional and radiative processes are insufficient in the IGM at relevant redshifts to couple $^3He^+$ to T_k or T_α, and, thus, $T_s \approx T_{CMB}$. Since T_s does not decouple significantly from T_{CMB} at relevant densities ($T_s \lesssim 2\,T_{CMB}$ for $\Delta_b < 100$ at $z = 3.6$), detecting intergalactic $^3He^+$ 8.7 GHz emission from this era would require a mammoth effort, but the $^3He^+$ 8.7 GHz line may be observable in absorption along the sightline to bright quasars with present and upcoming instruments.

An obvious science application of $^3He^+$ hyperfine absorption is to study He II reionization. This process is believed to occur at lower redshift than hydrogen reionization, with several lines of evidence indicating that it completes by $z \sim 3$. However, all present observations that claim a detection of He II reionization are controversial because of their indirect nature. The most direct present-day probe of this process is the He II Lyα forest, but this absorption saturates at He II fractions of 10^{-3} at the cosmic mean density.

In contrast, intergalactic hyperfine absorption of $^3He^+$ is a linear tracer of the product of the density and the fraction of helium that is He II. This absorption against the brightest sources at $z \sim 4$ (which have $S \sim 1$ Jy) creates ~ 1 μJy fluctuations on $\gtrsim 0.1$ MHz scales. While such sensitivities are beyond the reach of present-day interferometers, we showed that a 10^5 m^2 instrument operating at its thermal limit could directly resolve these fluctuations, and the SKA could potentially image these fluctuations with high signal to noise.

A key insight that reduces the sensitivity requirements for detection is that H I Lyα forest absorption at optical wavelengths can be used to locate the spectral bins with large values of $\tau_{^3He^+}$ (in overdensities). Using this information to stack pixels in a radio observation, one can statistically detect 8.7 GHz absorption with an RMS noise of $\sim 30\,\mu$Jy in 0.1 MHz spectral bands over 100 MHz ($\Delta z \approx 0.25$) on a 1 Jy source. These sensitivity requirements may be within the reach of present interferometers.

Furthermore, at $z \lesssim 3$ current instruments may be able to study $^3He^+$ absorption in systems that are self-shielded to He II-ionizing photons against the brightest radio sources on the sky. Estimates are that there are ~ 10 such systems per 100 MHz, and H I Lyα forest information can also be exploited to stack such systems. At present, there is considerable uncertainty with modeling 8.7 GHz absorption from the most dense systems ($N_{HI} \gtrsim 10^{18}$ cm^{-2}), and further study is required to understand how much absorption is expected. However, the densest systems, which will appear as DLAs in the Lyα forest, could have $\tau_{^3He^+} \sim 10^{-4}$.

Another application of intergalactic 8.7 GHz absorption is to constrain the primordial ^{3}He abundance. To achieve such a constraint, an interferometer would target intergalactic He II regions along skewers, and from these directly measure the abundance of ^{3}He, analogously to how Ω_b is measured from the H I Lyα forest. Such observations would need to image the signal ($\sim \mu$Jy sensitivities in ~ 1 MHz spectral bins). The primordial ^{3}He abundance is currently constrained by observations of galactic H II regions, which involves detailed modeling of the H II region lines and is also uncertain to the extent stellar nucleosynthesis effects the abundance in these regions. An intergalactic measurement of the ^{3}He abundance does not suffer from these uncertainties and, therefore, could be more decisive.

Finally, an even more ambitious project would be to use this absorption to study the reionization of the first electron of helium, which is thought to occur at the same time as the reionization of hydrogen. To study the reionization of the first electron of helium using 8.7 GHz absorption with the SKA would require a ~ 50 mJy source at $z > 6$ to image this signal (assuming perfect instrumental calibration and $T_{sys} = 20$ K). Source populations at high-redshift are very uncertain, but we argued that it is possible that such sources exist. Low-redshift 21 cm emission falls in the same band and can contaminate such observations. However, an interferometric measurement with $\gtrsim 1$ km baselines should be able to avoid significant contamination from this foreground.

Further study of precision wideband spectrometry in this (super-21 cm) range may prove worthwhile. The dominant radiation at these frequencies is the well-characterized CMB such that it may be possible to isolate interesting foreground signals. Potential observables in this band include other intergalactic hyperfine lines [68], molecular and fine-structure lines from the first galaxies [72, 73], and spectral distortions produced during cosmological recombination [74].

Acknowledgments

M.M. and E.S. contributed equally to the writing and calculations presented in this study. We would like to thank Chris Hirata and Steve Furlanetto for

useful comments on the manuscript. We acknowledge discussions with Hsiao-Wen Chen, Simon DeDeo, Mark Dijkstra, C.-A. Faucher-Giguère, Lars Hernquist, Chris Hirata, Adam Lidz, Ann Mao, Daniel Marrone, Jeff McMahon, Kenneth Nollett, Brant Robertson, and Matias Zaldarriaga. E.S. thanks participants of the workshop, "The Physics of Cosmological Recombination" for discussion and stimulating study of signals in this frequency range, and is, in particular, grateful to Chris Hirata for suggesting $^3He^+$ in the context of the recombination spectral distortions. M.M. acknowledges support from the NSF. E.S. acknowledges support by NSF Physics Frontier Center grant PHY-0114422 to the Kavli Institute of Cosmological Physics.

While this project was nearing completion, we learned of a similar effort on 3He+ hyperfine emission by Bagla and Loeb [75]. We refer the reader there for complementary discussion.

Appendix A: Additional spin temperature-coupling processes

In addition to collisional and radiative processes, there are four other processes which are subdominant: 1) magnetic dipole interaction with a passing electron, and interactions between the proton spin and a passing electron 2) bound-free and free-bound processes, 3) collisions that drive electronic state transitions or resonant scattering, and 4) charge exchange [28]. However, the magnetic dipole interaction between the ionic electron and passing electron as well as the interaction between the proton and passing electron is negligible [37]. Thermal electron capture at low Z is also subdominant to the thermal spin exchange [76].

Electronic excitation of the $^3He^+$ from a passing electron can perform a similar role as radiative spin pumping. To excite $1s \to 2p$, one needs $E_{\rm th} = (3/4)Z^2 E_{\rm Ry} \approx 40.8$ eV $\gg k_{\rm B}T_{\rm k}$ (where $E_{\rm Ry} = 13.6$ eV), which is clearly scarce at relevant temperatures of $\sim 10^4$ K. Additionally, an electron can scatter resonantly through an intermediate state. Here, the passing electron becomes temporarily bound, introducing $E_{\rm free} + E_{\rm binding}$ to excite the ground state. We follow [28] in estimating the contribution from this process. First consider the impact excitation for a free electron. Here, the cross section is relatively flat above threshold $E_{\rm th}$ [77], and

$$\begin{aligned}\bar{\sigma}_{\rm 1s-2p} &= \frac{1}{(k_{\rm B}T_{\rm k})^2}\int_{E_{\rm th}}^{\infty} dE\sigma(E)Ee^{-E/(k_{\rm B}T_{\rm k})} \\ &\approx \frac{9\ {\rm eV}}{k_{\rm B}T_{\rm k}} a_o^2 e^{-E{\rm th}/(k_{\rm B}T_{\rm k})}. \end{aligned} \quad \text{(A1)}$$

The resonant (intermediate bound state) form of this process is roughly boosted by $\exp(Z^2E_{\rm Ry}/(4k_{\rm B}T_{\rm k})$. This is still clearly insufficient at IGM temperatures (where $k_{\rm B}T_{\rm k} \approx 1$ eV $\ll (2/3)E_{\rm th}$) to boost the spin exchange rate.

In charge exchange, $He^+ + H \leftrightarrow He + H^+ + \gamma$. The forward rate gives an upper bound on the spin exchange through this mechanism, and is [78]

$$\frac{\dot{x}_{\rm HeII}}{x_{\rm HeII}} \approx -(1\times 10^{-15}\ {\rm cm}^3 s^{-1})\left(\frac{T_{\rm k}}{300\ {\rm K}}\right)^{1/4} n_H x_{\rm HI}, \quad \text{(A2)}$$

which, during this era, is $\sim 10^{-24}$ s^{-1}, and so is also negligible. In addition, charge exchange with atoms other than H should be even more negligible.

Appendix B: Electron-^{3}He+ scattering

Here, we consider the spin exchange from electron-$^3He^+$ collisions (described in Sec. II B 1) in more detail. For an incident plane wave, the output wave has an unscattered and a scattered component [37],

$$\Psi_{\rm out} \propto e^{ikx} + f_k(\theta)\frac{e^{ikr}}{r}, \quad \text{(B1)}$$

such that the differential cross section is $d\sigma/d\Omega = |f_k(\theta)|^2$. We index the spin state using bra-ket notation with placeholders nuclear spin, comma, atomic electron spin, scattering electron spin. In analogy to [41], but applied to $^3He^+$, the atomic wavefunction for the singlet excited state is $\psi_H/\sqrt{2}[|\uparrow,\downarrow\cdot\rangle - |\downarrow,\uparrow\cdot\rangle]$ where ψ_H is the space part of the wave function. An unpolarized incident electron has wavefunction $e^{ikx}/\sqrt{2}[e^{i\gamma}|\cdot,\cdot\uparrow\rangle + |\cdot,\cdot\downarrow\rangle]$. The combined spin space of the incident electron and singlet-state atom that will produce a spin exchange is $\psi_H e^{ikx}/2[e^{i\gamma}|\uparrow,\downarrow\uparrow\rangle - |\downarrow,\uparrow\downarrow\rangle]$. We can write the electron-electron component of the interaction as the sum of triplet and singlet states, $|\uparrow,\downarrow\uparrow\rangle = \frac{1}{2}[(|\uparrow,\downarrow\uparrow\rangle + |\uparrow,\uparrow\downarrow\rangle) - (|\uparrow,\uparrow\downarrow\rangle - |\uparrow,\downarrow\uparrow\rangle)]$. Through the interaction, though, the electron-electron singlet and triplet will be mapped differently to output states as

$$\begin{aligned}|\uparrow,\downarrow\uparrow\rangle \ \mapsto\ & \frac{1}{2}[T(\theta)(|\uparrow,\downarrow\uparrow\rangle + |\uparrow,\uparrow\downarrow\rangle) \\ & - S(\theta)(|\uparrow,\uparrow\downarrow\rangle - |\uparrow,\downarrow\uparrow\rangle)], \end{aligned} \quad \text{(B2)}$$

and analogously for $|\downarrow,\uparrow\downarrow\rangle$. Here, $T(\theta)$ and $S(\theta)$ describe scattering through angle θ between the asymptotic in and out states in the momentum basis. If we now find the matrix element to the final state $m_F = 1$ of the $F = 1$ atomic triplet output state $\langle\uparrow,\uparrow\cdot|$ to get the scattering part of the matrix element

$$\frac{e^{ikr}\psi_H}{4r}[e^{i\gamma}(T(\theta)-S(\theta))|\cdot,\cdot\downarrow\rangle] \Rightarrow \frac{d\sigma}{d\Omega} = \frac{1}{2^4}|T(\theta)-S(\theta)|^2. \quad \text{(B3)}$$

(Note that this calculation simplifies the wave functions to anticipate terms that contribute to the $m_F = 1$ or $m_F = -1$ final state cross sections [41]. The restriction to spin-flip wavefunctions does not apply to $m_F = 0$.)

Expand T and S identically in the partial wave basis as [79]

$$T(\theta) = \frac{1}{2ik}\sum_{\ell}(2\ell+1)[e^{2i\delta_\ell^t}-1]P_\ell(\cos(\theta)). \quad \text{(B4)}$$

This relates the momentum space representation of $T(\theta)$ and $S(\theta)$ to an angular momentum basis in which the scattering matrix is diagonal, making unitarity manifest through real phase shifts δ_ℓ^s and δ_ℓ^t. Integrating $d\sigma/d\Omega$ over angle and using the orthogonality of the Legendre polynomials gives

$$\sigma = \frac{\pi}{4k^2}\sum_{\ell}(2\ell+1)\sin^2(\delta_\ell^t-\delta_\ell^s). \quad \text{(B5)}$$

Taking the total cross section to any of the triplet state produces the factor of 3 in Eq. 7.

To evaluate σ, we use the calculated values for the phase shifts in [36]. However, even without knowledge of these values, one can derive a unitarity bound assuming that s-wave scattering dominates. Note that s-wave scattering dominates the spin-exchange cross section at relevant energies [37]. Since $\sin^2(\delta_0^t-\delta_0^s)<1$, this yields the bound

$$\sigma < \frac{3\pi}{4k^2} \Rightarrow \bar{\sigma} < \frac{3\pi}{4}\frac{13.6\text{ eV}}{k_BT}a_o^2. \quad \text{(B6)}$$

This bound is only 30% larger than our more detailed estimate for $\bar{\sigma}$ (Eq. 8).

All of the interaction physics in our calculation of σ is hidden in δ_l^t and δ_l^s. Employing a more physically complete approach, Augustin et al. [76] decomposed the scattering matrix into a direct (Rutherford) Coulomb scattering term and an exchange term. They then proceeded to evaluate the exchange term using the Coulomb wave function for the scattering electron. They found that $\sigma \propto Z^{-2}/E$ for hydrogen-like ions, where Z is the nuclear charge. Thus, the effectiveness of spin exchange decreases with nuclear charge.

[1] C. L. Carilli, N. Y. Gnedin, and F. Owen, Astrophys. J. **577**, 22 (2002), arXiv:astro-ph/0205169.
[2] S. R. Furlanetto and A. Loeb, Astrophys. J. **579**, 1 (2002), arXiv:astro-ph/0206308.
[3] S. R. Furlanetto, Mon. Not. R. Astron. Soc. **370**, 1867 (2006), arXiv:astro-ph/0604223.
[4] H. A. Schuessler, E. N. Fortson, and H. G. Dehmelt, Physical Review **187**, 5 (1969).
[5] H. C. Goldwire, Jr. and W. M. Goss, Astrophys. J. **149**, 15 (1967).
[6] R. J. Gould, Astrophys. J. **423**, 522 (1994).
[7] S. R. Furlanetto and S. P. Oh, Astrophys. J. **681**, 1 (2008), 0711.1542.
[8] S. R. Furlanetto and S. P. Oh, Astrophys. J. **682**, 14 (2008), 0711.0751.
[9] S. R. Furlanetto, Z. Haiman, and S. P. Oh, Astrophys. J. **686**, 25 (2008), 0803.3454.
[10] M. McQuinn, A. Lidz, M. Zaldarriaga, L. Hernquist, P. F. Hopkins, S. Dutta, and C.-A. Faucher-Giguère, Astrophys. J. **694**, 842 (2009), 0807.2799.
[11] A. V. Belikov and D. Hooper, ArXiv e-prints (2009), 0904.1210.
[12] M. Volonteri and N. Gnedin, ArXiv e-prints (2009), 0905.0144.
[13] M. Ricotti, N. Y. Gnedin, and J. M. Shull, Astrophys. J. **534**, 41 (2000), arXiv:astro-ph/9906413.
[14] J. Schaye, T. Theuns, M. Rauch, G. Efstathiou, and W. L. W. Sargent, Mon. Not. R. Astron. Soc. **318**, 817 (2000), arXiv:astro-ph/9912432.
[15] S. R. Heap, G. M. Williger, A. Smette, I. Hubeny, M. S. Sahu, E. B. Jenkins, T. M. Tripp, and J. N. Winkler, Astrophys. J. **534**, 69 (2000).
[16] M. McQuinn, ArXiv e-prints (2009), 0905.0481.
[17] A. Songaila, Astron. J. **115**, 2184 (1998), arXiv:astro-ph/9803010.
[18] I. I. Agafonova, M. Centurión, S. A. Levshakov, and P. Molaro, Astron. Astrophys. **441**, 9 (2005), arXiv:astro-ph/0506138.
[19] K. A. Olive, R. T. Rood, D. N. Schramm, J. Truran, and E. Vangioni-Flam, Astrophys. J. **444**, 680 (1995), arXiv:astro-ph/9410058.
[20] R. T. Rood, T. M. Bania, D. S. Balser, and T. L. Wilson, Space Science Reviews **84**, 185 (1998).
[21] E. Komatsu, J. Dunkley, M. R. Nolta, C. L. Bennett, B. Gold, G. Hinshaw, N. Jarosik, D. Larson, M. Limon, L. Page, et al., Astrophys. J. Supp. **180**, 330 (2009), 0803.0547.
[22] P. P. Eggleton, D. S. P. Dearborn, and J. C. Lattanzio, Astrophys. J. **677**, 581 (2008).
[23] D. S. Balser, R. T. Rood, and T. M. Bania, Science **317**, 1171 (2007).
[24] R. A. Syunyaev, Astronomicheskii Zhurnal **43**, 1237 (1966).
[25] K. Sigurdson and S. R. Furlanetto, Physical Review Letters **97**, 091301 (2006), arXiv:astro-ph/0505173.
[26] S. R. Furlanetto, S. P. Oh, and F. H. Briggs, Phys. Rep. **433**, 181 (2006), arXiv:astro-ph/0608032.
[27] R. A. Sunyaev and D. O. Docenko, Astronomy Letters **33**, 67 (2007), arXiv:astro-ph/0608256.
[28] R. A. Sunyaev and E. M. Churazov, Soviet Astronomy Letters **10**, 201 (1984).
[29] M. Bersanelli, G. F. Smoot, M. Bensadoun, G. de Amici, M. Limon, and S. Levin, Astrophysical Letters Communications **32**, 7 (1995).
[30] S. G. Karshenboim, N. N. Kolachevsky, V. G. Ivanov, M. Fischer, P. Fendel, and T. W. Hänsch, Soviet Journal of Experimental and Theoretical Physics **102**, 367 (2006).
[31] M. Zaldarriaga, S. R. Furlanetto, and L. Hernquist, Astrophys. J. **608**, 622 (2004), arXiv:astro-ph/0311514.
[32] J. Schaye, Astrophys. J. **559**, 507 (2001), arXiv:astro-ph/0104272.

[33] C.-A. Faucher-Giguère, A. Lidz, L. Hernquist, and M. Zaldarriaga, Astrophys. J. Lett. **682**, L9 (2008), 0806.0372.

[34] G. B. Field, Astrophys. J. **129**, 536 (1959).

[35] M. Seiffert, D. J. Fixsen, A. Kogut, S. M. Levin, M. Limon, P. M. Lubin, P. Mirel, J. Singal, T. Villela, E. Wollack, et al., ArXiv e-prints (2009), 0901.0559.

[36] P. Khan, M. Daskhan, A. S. Ghosh, and C. Falcon, Phys. Rev. A **26**, 1401 (1982).

[37] S. R. Furlanetto and M. R. Furlanetto, Mon. Not. R. Astron. Soc. **374**, 547 (2007), arXiv:astro-ph/0608067.

[38] L. Chuzhoy and P. R. Shapiro, Astrophys. J. **651**, 1 (2006), arXiv:astro-ph/0512206.

[39] C. M. Hirata, Mon. Not. R. Astron. Soc. **367**, 259 (2006), arXiv:astro-ph/0507102.

[40] J. R. Pritchard and S. R. Furlanetto, Mon. Not. R. Astron. Soc. **367**, 1057 (2006), arXiv:astro-ph/0508381.

[41] G. B. Field, Proc. I.R.E. **46**, 240 (1958).

[42] X. Chen and J. Miralda-Escudé, Astrophys. J. **602**, 1 (2004), arXiv:astro-ph/0303395.

[43] S. Deguchi and W. D. Watson, Astrophys. J. **290**, 578 (1985).

[44] J. Miralda-Escude, Astrophys. J. **501**, 15 (1998), arXiv:astro-ph/9708253.

[45] D. E. Osterbrock, *Astrophysics of gaseous nebulae and active galactic nuclei* (1989).

[46] C. . Faucher-Giguere, A. Lidz, M. Zaldarriaga, and L. Hernquist, ArXiv e-prints (2009), 0901.4554.

[47] J. Miralda-Escudé, M. Haehnelt, and M. J. Rees, Astrophys. J. **530**, 1 (2000), arXiv:astro-ph/9812306.

[48] I. M. Hook, R. G. McMahon, P. A. Shaver, and I. A. G. Snellen, Astron. Astrophys. **391**, 509 (2002), arXiv:astro-ph/0207101.

[49] M. Vigotti, R. Carballo, C. R. Benn, G. De Zotti, R. Fanti, J. I. Gonzalez Serrano, K.-H. Mack, and J. Holt, Astrophys. J. **591**, 43 (2003), arXiv:astro-ph/0303333.

[50] M. J. Drinkwater, R. L. Webster, P. J. Francis, J. J. Condon, S. L. Ellison, D. L. Jauncey, J. Lovell, B. A. Peterson, and A. Savage, Mon. Not. R. Astron. Soc. **284**, 85 (1997), arXiv:astro-ph/9609019.

[51] R. Carballo, J. I. González-Serrano, F. M. Montenegro-Montes, C. R. Benn, K.-H. Mack, M. Pedani, and M. Vigotti, Mon. Not. R. Astron. Soc. **370**, 1034 (2006), arXiv:astro-ph/0605298.

[52] W. van Breugel, C. De Breuck, S. A. Stanford, D. Stern, H. Röttgering, and G. Miley, Astrophys. J. Lett. **518**, L61 (1999), arXiv:astro-ph/9904272.

[53] C. L. Carilli, R. Wang, M. B. van Hoven, K. Dwarakanath, J. N. Chengalur, and S. Wyithe, Astron. J. **133**, 2841 (2007), arXiv:astro-ph/0703797.

[54] P. G. Edwards and S. J. Tingay, Astron. Astrophys. **424**, 91 (2004), arXiv:astro-ph/0407010.

[55] A. Omar, K. R. Anantharamaiah, M. Rupen, and J. Rigby, Astron. Astrophys. **381**, L29 (2002), arXiv:astro-ph/0111268.

[56] W. H. Press and G. B. Rybicki, Astrophys. J. **418**, 585 (1993), arXiv:astro-ph/9303017.

[57] T. Theuns, A. Leonard, G. Efstathiou, F. R. Pearce, and P. A. Thomas, Mon. Not. R. Astron. Soc. **301**, 478 (1998), arXiv:astro-ph/9805119.

[58] M. A. Zwaan, L. Staveley-Smith, B. S. Koribalski, P. A. Henning, V. A. Kilborn, S. D. Ryder, D. G. Barnes, R. Bhathal, P. J. Boyce, W. J. G. de Blok, et al., Astron. J. **125**, 2842 (2003), arXiv:astro-ph/0302440.

[59] R. Fonseca, D. Barbosa, L. Cupido, A. Mourão, D. M. Dos Santos, G. F. Smoot, and C. Tello, New Astronomy **11**, 551 (2006), arXiv:astro-ph/0411477.

[60] M. McQuinn, O. Zahn, M. Zaldarriaga, L. Hernquist, and S. R. Furlanetto, Astrophys. J. **653**, 815 (2006), arXiv:astro-ph/0512263.

[61] M. Johnston-Hollitt, C. P. Hollitt, and R. D. Ekers, in *The Magnetized Interstellar Medium*, edited by B. Uyaniker, W. Reich, and R. Wielebinski (2004), pp. 13–18.

[62] Z.-W. Xu, J. Wu, and Z.-S. Wu, Waves in Random Media **14**, 189 (2004).

[63] S. P. Oh and K. J. Mack, Mon. Not. R. Astron. Soc. **346**, 871 (2003), arXiv:astro-ph/0302099.

[64] P. A. Shaver, Astron. Astrophys. **43**, 465 (1975).

[65] D. P. Finkbeiner, Astrophys. J. Supp. **146**, 407 (2003), arXiv:astro-ph/0301558.

[66] A. M. Wolfe, E. Gawiser, and J. X. Prochaska, Ann. Rev. Astron. Astrophys. **43**, 861 (2005), arXiv:astro-ph/0509481.

[67] I. Kazes, J. Crovisier, and D. Aubry, Astron. Astrophys. **58**, 403 (1977).

[68] C. H. Townes, in *Radio astronomy*, edited by H. C. van de Hulst (1957), vol. 4 of *IAU Symposium*, pp. 92–+.

[69] J. Darling, P. Goldsmith, D. Li, and R. Giovanelli, Astron. J. **125**, 1177 (2003), arXiv:astro-ph/0301314.

[70] J. P. Wild, Astrophys. J. **115**, 206 (1952).

[71] M. Dijkstra, A. Lidz, J. R. Pritchard, L. J. Greenhill, D. A. Mitchell, S. M. Ord, and R. B. Wayth, Mon. Not. R. Astron. Soc. **390**, 1430 (2008), 0809.4279.

[72] K. Basu, C. Hernández-Monteagudo, and R. A. Sunyaev, Astron. Astrophys. **416**, 447 (2004), arXiv:astro-ph/0311620.

[73] M. Righi, C. Hernández-Monteagudo, and R. A. Sunyaev, Astron. Astrophys. **489**, 489 (2008), 0805.2174.

[74] J. A. Rubiño-Martín, J. Chluba, and R. A. Sunyaev, Mon. Not. R. Astron. Soc. **371**, 1939 (2006), arXiv:astro-ph/0607373.

[75] J. S. Bagla and A. Loeb, ArXiv e-prints (2009), 0905.1698.

[76] J. Augustin, B. Müller, and W. Greiner, Zeitschrift fur Physik D Atoms Molecules Clusters **14**, 317 (1989).

[77] V. I. Fisher, Y. V. Ralchenko, V. A. Bernshtam, A. Goldgirsh, Y. Maron, L. A. Vainshtein, I. Bray, and H. Golten, Phys. Rev. A **55**, 329 (1997).

[78] P. C. Stancil, S. Lepp, and A. Dalgarno, Astrophys. J. **509**, 1 (1998).

[79] P. G. Burke and H. M. Schey, Physical Review **126**, 163 (1962).

[80] S. Deguchi, Astrophys. J. **291**, 492 (1985).

[81] L. Danese and R. B. Partridge, Astrophys. J. **342**, 604 (1989).

[82] The principle of the Wouthuysen-Field coupling is that, when photons scatter off of the $^3He^+$ resonances, each event has some probability to switch the hyperfine state of the ion. If sufficient scatterings take place, this scattering can couple the T_s to the color temperature of the radiation. In addition, energy exchange between the gas and He II Lyman-series photons tends to drive the color temperature around the resonance frequency to the gas temperature.

[83] Higher density regions could have synchrotron or free-free emission at 8.7 GHz in excess of T_{CMB}, but these regions likely already have $T_s \gg T_k$ anyway due to collisional

coupling.

[84] This can be derived from Eq. (23) in Field [41] noting that the level structure is the same as hydrogen, except that the singlet energies are above the triplet, which means that $P_{10}/P_{\alpha,^3\mathrm{He}^+}$ for $^3\mathrm{He}^+$ is the same as $P_{01}/P_{\alpha,H}$ for hydrogen, where P_{01} is the respective scattering excitation rate.

[85] Scattering in the wing of the Lyα line is significantly less important for $z \sim 3$ helium than $z > 6$ hydrogen because of its lower abundance, the lower densities at these redshifts, and a photon redshifts 4 times faster across the He II Lyα line.

[86] In a He II region He II Lyn photons are either locally scattered by ^{4}He+ and destroyed, which ≈ 0.3 of the time for $n > 2$ (0 of the time for $n = 1$) results in a Lyα photon that can pump the $^3\mathrm{He}^+$ (this fraction is included in the 0.7 in Eq. 12), or it will redshift until it reaches the next resonance before it has a chance of being converted to a He II Lyα photon. The contribution to pumping from photons produced by recombinations in He III regions would essentially be given by equation (12), but with the replacement $\langle \Delta_b^2 x_{\mathrm{HeIII}} \rangle \rightarrow 0.02\, \bar{\Delta}_b^2\ \bar{x}_{\mathrm{HeIII}}$, where 0.02 factor comes from the small probability of producing such photons in a recombination cascade and, then, the probability that these photons produce a He II Lyα photon.

[87] In addition, several of the $^3\mathrm{P}^0$–$2\mathrm{P}^2\ ^3\mathrm{P}$ resonances of O III are offset ~ 100 km s^{-1} blueward of the ^{3}He+ Lyα resonance. These resonances can destroy continuum photons [80], suppressing β_∞ even further.

[88] From their respective proposer's guides and overviews: for the GBT, we take 2 K/Jy; for the VLA, we take 0.098 K/Jy; for the GMRT, we take 0.22 K/Jy. All gains here are for a single antenna.

[89] For DLAs, most of the hydrogen should be self-shielded to ionizing photons such that the hydrogen gas is substantially neutral. Because of this, the ratio of N_{HI} to $N_{^3\mathrm{He}^+}$ will be smaller than for lower N_{HI} systems. However, the helium in H I regions will often stays in the He II state because the photoionization cross section for He I is a much flatter function of frequency than that of the H I. Thus, hard photons penetrate into H I regions and keep the helium singly ionized. An effect that suppresses the $^3\mathrm{He}^+$ absorption signal is that at particle densities of $n = 3 \times 10^{-3}\,\mathrm{cm}^{-3}$ in H II regions (and of $n = 4 \times 10^{-2}\,\mathrm{cm}^{-3}$ in H I regions) $T_{\mathrm{s}} = 2\,T_{\mathrm{CMB}}$. Henceforth, T_{s} increases approximately linearly with density such that $\tau_{^3\mathrm{He}^+}$ becomes independent of density.

[90] The FCC only formally allocates 1.66 GHz to 1.67 GHz to radio astronomy and experimental downlinks. For a survey of RFI at the GBT see L-band and S-band RFI studies under `http://www.gb.nrao.edu/IPG/`.

[91] The frequencies under consideration fall below the most notable molecular resonances in the atmosphere, and are well above the plasma frequency of the ionosphere, so these are both mild considerations compared to lower and higher-frequency experiments. In this frequency range, the atmosphere's effective temperature is ~ 1 K [29, 81] and is dominated by emission from molecular oxygen (which is very flat in frequency [81]), but depends on precipitable water vapor at the level of 1 mK/mm. Further, in the bulk of the atmosphere, pressure broadening wipes out spectral structure on the scales considered.

[92] Collisions that change the valence electron state between the nS and nP electronic states in non-hydrogen-like ions may efficiently pump these hyperfine lines at IGM densities [28], resulting in emission. Therefore, redshifted ^{14}NV may provide an important contribution to the diffuse background at ~ 2 GHz at the $\delta T_b \sim 10^{-7}$ K-level, assuming $\langle W \rangle = 0.1$.